JOC The Journal of Organic Chemistry

Article

pubs.acs.org/joc

Recognition of Mixed-Sequence DNA Duplexes: Design Guidelines for Invaders Based on 2′-*O*-(Pyren-1-yl)methyl-RNA Monomers

Saswata Karmakar, Dale C. Guenther, and Patrick J. Hrdlicka*

Department of Chemistry, University of Idaho, 875 Perimeter Drive, MS 2343, Moscow, Idaho 83844-2343, United States

Supporting Information

ABSTRACT: The development of agents that recognize mixed-sequence double-stranded DNA (dsDNA) is desirable because of their potential as tools for detection, regulation, and modification of genes. Despite progress with triplex-forming oligonucleotides, peptide nucleic acids, polyamides, and other approaches, recognition of mixed-sequence dsDNA targets remains challenging. Our laboratory studies *Invaders* as an alternative approach toward this end. These double-stranded oligonucleotide probes are activated for recognition of mixed-sequence dsDNA through modification with +1 interstrand zippers of intercalator-functionalized nucleotides such as 2′-*O*-(pyren-1-yl)methyl-RNA monomers and have recently been shown to recognize linear dsDNA, DNA hairpins, and chromosomal DNA. In the present work, we systematically studied the influence that the nucleobase moieties of the 2′-*O*-(pyren-1-yl)methyl-RNA monomers have on the recognition efficiency of Invader duplexes. Results from thermal denaturation, binding energy, and recognition experiments using Invader duplexes with different +1 interstrand zippers of the four canonical 2′-*O*-(pyren-1-yl)methyl-RNA **A**/**C**/**G**/**U** monomers show that incorporation of these motifs is a general strategy for activation of probes for recognition of dsDNA. Probe duplexes with interstrand zippers comprising **C** and/or **U** monomers result in the most efficient recognition of dsDNA. The insight gained from this study will drive the design of efficient Invaders for applications in molecular biology, nucleic acid diagnostics, and biotechnology.

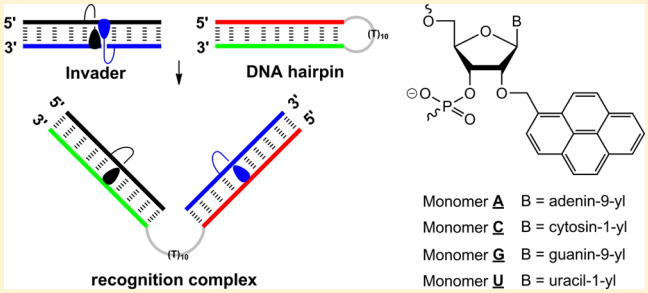

INTRODUCTION

The development of compounds that recognize double-stranded DNA (dsDNA) in a sequence-specific manner is a research area of considerable interest that is motivated by the prospect for molecular tools that can detect, regulate, and modify genes.[1−3] Significant advances have been made with triplex-forming oligonucleotides,[4−6] peptide nucleic acids (PNAs),[7,8] polyamides,[9,10] pseudocomplementary PNA,[11−13] γ-PNA,[14,15] engineered proteins,[16,17] and other approaches.[18−26] However, the development of alternative strategies for specific mixed-sequence recognition of dsDNA under physiological conditions remains a very desirable goal because of the limitations of current probe technologies, which include target sequence restrictions, insufficient binding affinity, need for low-salinity conditions, poor cellular uptake, and/or challenging synthesis.

Our laboratory is exploring so-called *Invaders* as an alternative strategy for mixed-sequence recognition of dsDNA.[27−31] These double-stranded oligonucleotide probes are activated for dsDNA recognition through modification with one or more +1 interstrand zipper arrangements of intercalator-modified nucleotide monomers such as 2′-*O*-(pyren-1-yl)-methyl-RNA monomers (Figure 1; for a formal definition of the zipper terminology, see the Experimental Section). Presumably, the intercalating pyrene moieties are forced into the same region of the duplex core, which causes a violation of the "nearest-neighbor exclusion principle",[32] resulting in concomitant localized unwinding and destabilization of the duplex (i.e., the formation of an "energetic hotspot"; Figure 1). The two strands that constitute an Invader duplex, on the other hand, display very strong affinity toward complementary single-stranded DNA (ssDNA), as duplex formation results in strongly stabilizing interactions between the pyrene and flanking nucleobases (Figure 1).[27−31] We have recently demonstrated that the stability difference between Invader probes and probe−target complexes can be used to realize mixed-sequence recognition of (i) linear dsDNA,[27,28,30] (ii) DNA hairpins,[29,31] and (iii) chromosomal DNA.[29]

In the present work, we systematically studied the influence that the nucleobase moieties of the 2′-*O*-(pyren-1-yl)methyl-RNA monomers, used to construct hotspots, have on the dsDNA recognition efficiency of Invader duplexes. It is important to gain this insight, as it will guide the future design of Invader duplexes for applications in molecular biology, nucleic acid diagnostics, and biotechnology.

RESULTS AND DISCUSSION

Synthesis of 2′-*O*-(Pyren-1-yl)methyl-RNA Phosphoramidites. The corresponding phosphoramidites of monomers

Received: September 20, 2013
Published: November 6, 2013

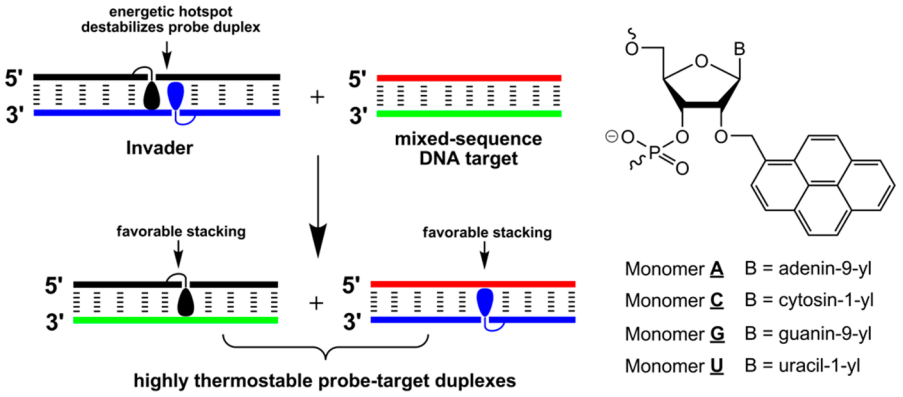

Figure 1. Illustration of the Invader concept for recognition of mixed-sequence dsDNA (droplets denote intercalating pyrene moieties) and structures of the monomers used in this study.

Scheme 1. Synthesis of 2′-*O*-(Pyren-1-yl)methyl-RNA-G^{iBu} Phosphoramidite 5[a]

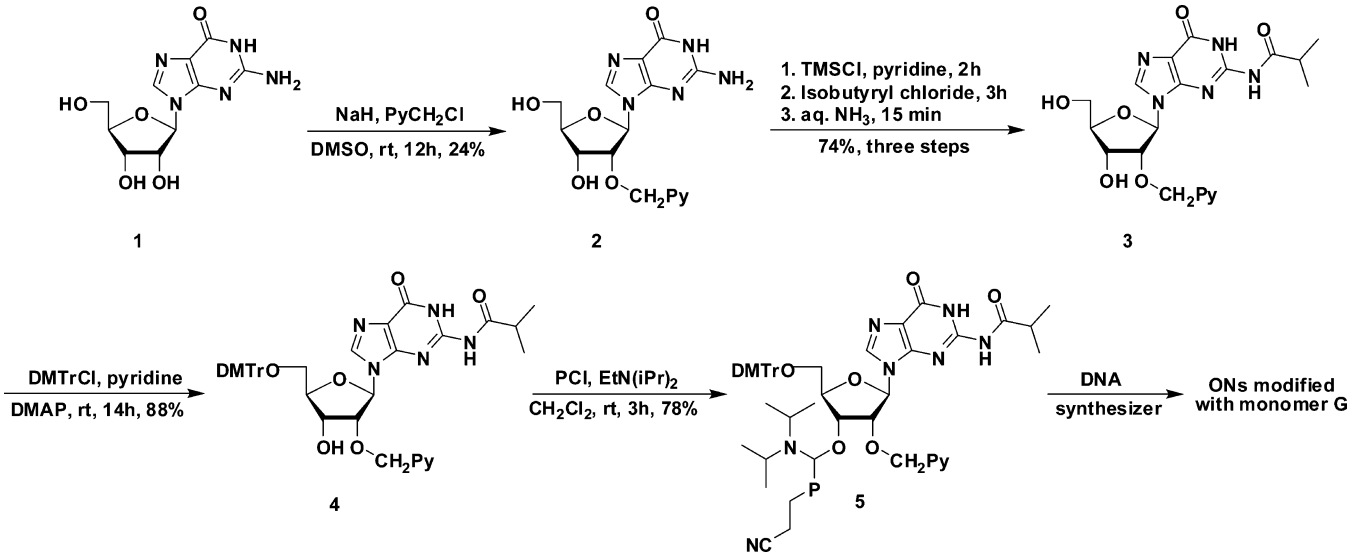

[a]Py = pyren-1-yl; TMSCl = trimethylsilyl chloride; DMTrCl = 4,4′-dimethoxytrityl chloride; PCl = 2-cyanoethyl-*N*,*N*-diisopropylchlorophosphoramidite.

A,[33] C,[33] and U[34] were synthesized as previously described. The novel N2-isobutyryl-protected 2′-*O*-(pyren-1-yl)-methylguanosine phosphoramidite **5** was obtained from guanosine (**1**) following the same general strategy that was used by others for the synthesis of the corresponding A^{Bz} and C^{Bz} phosphoramidites (Scheme 1).[33] Thus, unprotected guanosine was treated with 1-chloromethylpyrene in the presence of sodium hydride, which afforded O2′-alkylated nucleoside **2** in a low but consistent yield (24%). The low yield is due to concomitant formation of O3′/O5′/N3′-alkylated products (results not shown). The following N2-isobutyryl protection of the nucleobase to give **3** was accomplished in 74% yield using a transient protection protocol.[35] Subsequent O5′-dimethoxytritylation afforded nucleoside **4** in 88% yield, which upon treatment with 2-cyanoethyl-*N*,*N*-diisopropylchlorophosphoramidite and Hünig's base provided the target phosphoramidite **5** in 78% yield. The disappearance of ^{1}H NMR signals from exchangeable protons upon D_2O addition, along with results from other one- and two-dimensional NMR experiments and high-resolution MALDI-MS, confirmed the proposed structures of nucleosides **2**–**5**. The modified phosphoramidites were used to incorporate monomers A/C/G/U into oligodeoxyribonucleotides (ONs) using machine-assisted solid-phase DNA synthesis (4,5-dicyanoimidazole as the activator, 15 min) in ~98% stepwise coupling yield.

Design of the Study. In order to systematically study the influence that hotspot composition has on the dsDNA recognition efficiency of Invader duplexes, we designed 10 model probes that vary only in the nature of the central hotspot (see Table 1). The inherent symmetry of the energetic hotspots along with the utilized sequence context (i.e., hotspots flanked by A:T pairs on either side) allowed us to study the 16 possible hotspot designs using 10 probes.

DNA Hybridization Characteristics of ONs Modified with 2′-*O*-(Pyren-1-yl)methyl-RNA Monomers. Virtually all of the individual Invader strands display strongly increased affinity toward—and increased duplex stability with—complementary single-stranded DNA compared with unmodified ONs (ΔT_m up to +13.0 °C, as shown in the first two ΔT_m columns in Table 1; $\Delta\Delta G^{293}$ values down to −15 kJ/mol, as shown in the first two ΔG^{293} two columns in Table 2). Interestingly, the G monomer has a considerably smaller stabilizing effect than the other 2′-*O*-(pyren-1-yl)methyl-RNA monomers and is even destabilizing in some cases [ΔT_m = 3–9 °C and $\Delta\Delta G^{293}$ = 3–

dx.doi.org/10.1021/jo402085v | J. Org. Chem. 2013, 78, 12040−12048

Table 1. Thermal Denaturation Temperatures (T_m) and Deviation of Additivity (DA) Values of 9-Mer DNA Duplexes Modified with 2′-*O*-(Pyren-1-yl)methyl-RNA Monomers[a]

		T_m [ΔT_m] (°C)				
ON	sequence	upper strand vs ssDNA	lower strand vs ssDNA	Invader duplex	dsDNA	DA (°C)
ON1 **ON20**	5′-GTGA **A**C TGC 3′-CACT T**G** ACG	42.0 [+6.5]	34.5 [−1.0]	24.0 [−11.5]	35.5	−17.0
ON2 **ON19**	5′-GTGA **A**G TGC 3′-CACT T**C** ACG	46.0 [+8.5]	42.5 [+5.0]	32.5 [−5.0]	37.5	−18.5
ON3 **ON18**	5′-GTGA **A**T TGC 3′-CACT T**A** ACG	40.0 [+8.5]	38.5 [+7.0]	25.0 [−6.5]	31.5	−22.0
ON4 **ON17**	5′-GTGA **C**A TGC 3′-CACT G**U** ACG	48.5 [+13.0]	45.5 [+10.0]	35.5 [±0.0]	35.5	−23.0
ON5 **ON16**	5′-GTGA **C**C TGC 3′-CACT G**G** ACG	46.0 [+6.5]	45.0 [+5.5]	33.0 [−6.5]	39.5	−18.5
ON6 **ON15**	5′-GTGA **C**G TGC 3′-CACT G**C** ACG	54.5 [+11.0]	53.5 [+10.0]	41.5 [−2.0]	43.5	−23.0
ON7 **ON14**	5′-GTGA **G**A TGC 3′-CACT C**U** ACG	42.0 [+6.5]	39.0 [+3.5]	26.0 [−9.5]	35.5	−20.0
ON8 **ON13**	5′-GTGA **G**C TGC 3′-CACT C**G** ACG	40.0 [−3.5]	38.0 [−5.5]	26.0 [−17.5]	43.5	−8.5
ON9 **ON12**	5′-GTGA **U**A TGC 3′-CACT A**U** ACG	42.5 [+13.0]	42.5 [+13.0]	26.5 [−3.0]	29.5	−29.0
ON10 **ON11**	5′-GTGA **U**T TGC 3′-CACT A**A** ACG	37.5 [+6.0]	42.5 [+11.0]	26.5 [−5.0]	31.5	−22.0

[a] ΔT_m = change in T_m value relative to the corresponding unmodified reference duplex. T_m values were determined from the first derivative maxima of the thermal denaturation curves (A_{260} vs T) recorded in medium salt buffer ([Na^+] = 110 mM, [Cl^-] = 100 mM, pH 7.0 (NaH_2PO_4/Na_2HPO_4)) using a 1.0 μM concentration of each strand. DA = ΔT_m(Invader duplex) − ΔT_m(upper strand vs ssDNA) − ΔT_m(lower strand vs ssDNA). Example of DA calculation: $DA_{ON10:ON11}$ = ΔT_m(**ON10**:**ON11**) − ΔT_m(**ON10**:ssDNA) − ΔT_m(ssDNA:**ON11**) = −5.0 °C − 6.0 °C − 11.0 °C = −22.0 °C. A/C/G/*T* = adenin-9-yl/cytosin-1-yl/guanin-9-yl/thymin-1-yl DNA monomers. For the structures of **A**/**C**/**G**/**U**, see Figure 1.

Table 2. Changes in Gibbs Free Energy upon Duplex Formation (ΔG^{293}) and Binding Energies (ΔG^{293}_{rec}) of 9-Mer Invaders at 293 K[a]

		ΔG^{293} [$\Delta\Delta G^{293}$] (kJ/mol)				
ON	sequence	upper strand vs ssDNA	lower strand vs ssDNA	Invader duplex	dsDNA	ΔG^{293}_{rec} (kJ/mol)
ON1 **ON20**	5′-GTGA **A**C TGC 3′-CACT T**G** ACG	−51 ± 1 [−5]	−46 ± 0 [±0]	−37 ± 0 [+9]	−46 ± 0	−14
ON2 **ON19**	5′-GTGA **A**G TGC 3′-CACT T**C** ACG	−62 ± 1 [−15]	−50 ± 1 [−3]	−42 ± 0 [+5]	−47 ± 0	−23
ON3 **ON18**	5′-GTGA **A**T TGC 3′-CACT T**A** ACG	−48 ± 0 [−4]	−48 ± 0 [−4]	−39 ± 0 [+5]	−44 ± 0	−13
ON4 **ON17**	5′-GTGA **C**A TGC 3′-CACT G**U** ACG	−58 ± 0 [−12]	−56 ± 0 [−10]	−42 ± 0 [+4]	−46 ± 0	−26
ON5 **ON16**	5′-GTGA **C**C TGC 3′-CACT G**G** ACG	−56 ± 1 [−5]	−54 ± 0 [−3]	−41 ± 0 [+10]	−51 ± 1	−18
ON6 **ON15**	5′-GTGA **C**G TGC 3′-CACT G**C** ACG	−63 ± 1 [−8]	−64 ± 1 [−9]	−48 ± 1 [+7]	−55 ± 0	−24
ON7 **ON14**	5′-GTGA **G**A TGC 3′-CACT C**U** ACG	−50 ± 0 [−4]	−49 ± 1 [−3]	−39 ± 0 [+7]	−46 ± 0	−14
ON8 **ON13**	5′-GTGA **G**C TGC 3′-CACT C**G** ACG	−50 ± 1 [+4]	−48 ± 0 [+6]	−39 ± 1 [+15]	−54 ± 0	−5
ON9 **ON12**	5′-GTGA **U**A TGC 3′-CACT A**U** ACG	−55 ± 1 [−14]	−53 ± 1 [−12]	−38 ± 1 [+3]	−41 ± 1	−29
ON10 **ON11**	5′-GTGA **U**T TGC 3′-CACT A**A** ACG	−46 ± 1 [−3]	−54 ± 0 [−11]	−38 ± 1 [+5]	−43 ± 1	−19

[a] $\Delta\Delta G^{293}$ is measured relative to ΔG^{293} for unmodified DNA duplexes (dsDNA). ΔG^{293} values were determined via baseline fitting of thermal denaturation curves. ΔG^{293}_{rec} = ΔG^{293}(upper strand vs ssDNA) + ΔG^{293}(lower strand vs ssDNA) − ΔG^{293}(Invader duplex) − ΔG^{293}(dsDNA). "±" denotes standard deviation.

12 kJ/mol less favorable than for **A**/**C**/**U** monomers, as shown in Tables 1 and 2; only ONs with identical 3′-flanking nucleotides, e.g. **ON1**, **ON5**, **ON14**, and **ON13**, should be compared (vide infra)]. Absorbance spectra of single-stranded **ON1**−**ON20** and their duplexes with ssDNA were recorded to determine whether the low stability of **G**-modified duplexes is linked to differences in pyrene binding modes (Figure S2 in the Supporting Information). Small hybridization-induced bathochromic shifts of pyrene absorption maxima, consistent with increased interactions between pyrene and nucleobases and hence pyrene intercalation,[36] were generally observed for all of the ONs ($\Delta\lambda$ = 0−4 nm; Table 3). While **G**-modified ONs displayed slightly smaller bathochromic shifts, the results do not rule out pyrene intercalation as a likely binding mode. We speculate that the destabilizing effect of the **G** monomer is

dx.doi.org/10.1021/jo402085v | J. Org. Chem. 2013, 78, 12040−12048

Table 3. Absorption Maxima in the 300−400 nm Region for Single-Stranded ON1−ON20, the Corresponding Duplexes with ssDNA, and Invaders Comprising These ONs[a]

		λ_{max} [$\Delta\lambda$] (nm)				
ON	sequence	upper strand	lower strand	upper strand vs ssDNA	lower strand vs ssDNA	Invader duplex
ON1 **ON20**	5′-GTGA **A**C TGC 3′-CACT T**G** ACG	349	351	352 [+3]	352 [+1]	349
ON2 **ON19**	5′-GTGA **A**G TGC 3′-CACT T**C** ACG	349	349	352 [+3]	352 [+3]	350
ON3 **ON18**	5′-GTGA **A**T TGC 3′-CACT T**A** ACG	349	351	352 [+3]	352 [+1]	349
ON4 **ON17**	5′-GTGA **C**A TGC 3′-CACT G**U** ACG	352	352	352 [±0]	353 [+1]	344
ON5 **ON16**	5′-GTGA **C**C TGC 3′-CACT G**G** ACG	349	350	352 [+3]	352 [+2]	344
ON6 **ON15**	5′-GTGA **C**G TGC 3′-CACT G**C** ACG	349	348	352 [+3]	352 [+4]	345
ON7 **ON14**	5′-GTGA **G**A TGC 3′-CACT C**U** ACG	349	349	351 [+2]	352 [+3]	344
ON8 **ON13**	5′-GTGA **G**C TGC 3′-CACT C**G** ACG	349	351	351 [+2]	352 [+1]	343
ON9 **ON12**	5′-GTGA **U**A TGC 3′-CACT A**U** ACG	348	349	352 [+4]	352 [+3]	345
ON10 **ON11**	5′-GTGA **U**T TGC 3′-CACT A**A** ACG	348	349	351 [+3]	352 [+2]	345

[a]Conditions as described in footnote *a* of Table 1. T = 5 °C, 1.0 μM concentration of each strand.

instead linked to a weakening of the **G**:C base pair following pyrene intercalation.[37]

As has been previously observed for **U**-modified ONs,[38] the nucleotide flanking a 2′-*O*-(pyren-1-yl)methyl-RNA monomer on the 3′-side has a major influence on the duplex stability. Thus, the stabilizing effect of 2′-*O*-(pyren-1-yl)methyl-RNA monomers is greater when they are flanked by a 3′-purine (ΔT_m = 0−12 °C and $\Delta\Delta G^{293}$ = 3−11 kJ/mol more stabilizing than with 3′-flanking pyrimidines; e.g., compare ΔT_m and $\Delta\Delta G^{293}$ for **ON9**, **ON17**, **ON10**, and **ON14** in Tables 1 and 2). This finding is consistent with the 3′-directed intercalating binding mode that has been proposed for the pyrene moiety on the basis of NMR structures of **U**-modified DNA duplexes,[39] as the larger aromatic surface area of a 3′-purine likely facilitates stronger stacking interactions with the pyrene moiety.

Thermostability and Thermodynamics of Invader Duplexes. The influence on duplex stability upon incorporation of a second monomer can be additive, more than additive, or less than additive relative to a corresponding singly modified duplex. This is readily quantified in terms of T_m values by the "deviation from additivity" (DA), which is defined as $DA_{ON_X:ON_Y} \equiv \Delta T_m(\mathbf{ON}_X{:}\mathbf{ON}_Y) - \Delta T_m(\mathbf{ON}_X{:}ssDNA) - \Delta T_m(ssDNA{:}\mathbf{ON}_Y)$ or expressed in terms of ΔG^{293} by the term $\Delta G^{293}_{rec}(\mathbf{ON}_X{:}\mathbf{ON}_Y) = \Delta G^{293}(\mathbf{ON}_X{:}ssDNA) + \Delta G^{293}(ssDNA{:}\mathbf{ON}_Y) - \Delta G^{293}(\mathbf{ON}_X{:}\mathbf{ON}_Y) - \Delta G^{293}(dsDNA)$, where $\mathbf{ON}_X{:}\mathbf{ON}_Y$ is an Invader duplex with a +1 interstrand zipper arrangement of 2′-*O*-(pyren-1-yl)methyl-RNA monomers. ΔG^{293}_{rec} also serves as an estimate for the thermodynamic potential of Invader duplexes for recognition of isosequential dsDNA targets (vide infra).

In agreement with our preliminary results,[29−31] Invader duplexes are strongly destabilized relative to singly modified duplexes, irrespective of the monomers used to construct the energetic hotspot (DA ≪ 0 °C; Table 1). In fact, all of the studied Invader duplexes display lower T_m values than the corresponding unmodified dsDNAs (ΔT_m between −17.5 and 0.0 °C; see the "Invader duplex" column in Table 1). Evidently, the two 2′-*O*-(pyren-1-yl)methyl-RNA monomers influence each other and destabilize duplexes when placed in +1 interstrand zippers. This is corroborated by the steady-state fluorescence emission spectra of Invader duplexes, which generally feature pyrene−pyrene excimer signals at $\lambda_{em} \approx 490$ nm (Figure S7 in the Supporting Information), implying a coplanar arrangement of the pyrene moieties with an interplanar separation of ∼3.4 Å.[20,27,28,31,40−45]

Similar conclusions are reached on the basis of the thermodynamic data: (i) the formation of Invader duplexes is 3−15 kJ/mol less favorable than the formation of the corresponding reference DNAs (see the $\Delta\Delta G^{293}$ values in the "Invader duplex" column in Table 2) and (ii) the $\Delta\Delta G^{293}$ values of Invader duplexes are 5−29 kJ/mol less favorable than would be expected for additive contributions from the two 2′-*O*-(pyren-1-yl)methyl-RNA monomers (see the ΔG^{293}_{rec} values in Table 2). Invader duplex destabilization is dominated by unfavorable enthalpy ($\Delta\Delta H$ = 20−80 kJ/mol, results not shown), presumably as +1 interstrand monomer arrangements perturb stacking and/or nearby base pairing as a consequence of violating the "nearest-neighbor exclusion principle".[32] Arrangement of monomers in +1 interstrand zippers results in a localized region with one intercalator per base pair (Figure 1). Local perturbation of the duplex is further corroborated by the broad melting profiles (Figure S1 in the Supporting Information) and the blue-shifted pyrene absorption maxima observed for Invader duplexes ($\Delta\lambda$ = 1−9 nm relative to probe−target duplexes; Table 3), which are indicative of weaker pyrene−nucleobase interactions. Previous modeling and NMR studies of Invader duplexes based on the closely related 2′-*N*-(pyren-1-yl)methyl-2′-amino-α-L-LNA monomers also strongly suggested localized duplex perturbation.[31]

The specific nature of the energetic hotspot influences the relative magnitude of Invader duplex destabilization. Thus, Invaders with hotspots composed of **G** monomers are more destabilized relative to the corresponding unmodified dsDNA than Invader duplexes composed of other 2′-*O*-(pyren-1-yl)methyl-RNA monomers (see the ΔT_m and $\Delta\Delta G^{293}$ values of

dx.doi.org/10.1021/jo402085v | J. Org. Chem. 2013, 78, 12040−12048

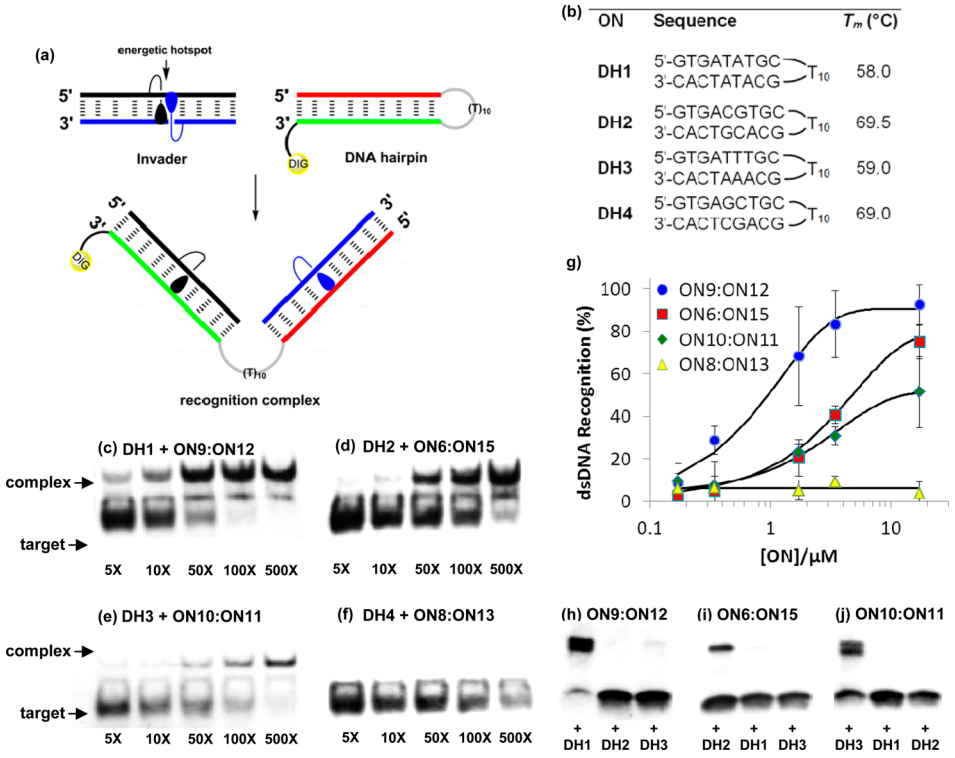

Figure 2. Invader-mediated recognition of DNA hairpins. (a) Illustration of the recognition process. (b) Sequences and T_m values of DNA hairpins with isosequential stems (conditions of thermal denaturation experiments; see Table 1). (c–f) Gel electropherograms illustrating dose–response experiments between (c) **DH1** and **ON9:ON12**, (d) **DH2** and **ON6:ON15**, (e) **DH3** and **ON10:ON11**, and (f) **DH4** and **ON8:ON13**. (g) Dose–response curves. (h–j) Gel electropherograms illustrating incubation of **DH1–DH3** with a 500-fold excess of **ON9:ON12**, **ON6:ON15**, or **ON10:ON11**, respectively. Experimental conditions: separately preannealed probes and targets (34.4 nM) were incubated for 15 h at room temperature in 1× HEPES buffer (50 mM HEPES, 100 mM NaCl, 5 mM $MgCl_2$, 10% sucrose, 1.4 mM spermine tetrahydrochloride, pH 7.2) and then run on 12 or 16% nondenaturing PAGE (performed at 70 V, 2 h, ~4 °C) using 0.5× TBE as a running buffer (45 mM Tris, 45 mM boric acid, 1 mM EDTA). DIG = digoxigenin.

ON1:ON20, **ON5:ON16**, **ON7:ON14**, and **ON8:ON13** in the "Invader duplex" columns in Tables 1 and 2).

Binding Energy for Invader-Mediated dsDNA Recognition. As mentioned above, the binding energy for recognition of isosequential dsDNA targets using Invader duplexes (i.e., the process depicted in Figure 1) is described by ΔG^{293}_{rec}; highly negative ΔG^{293}_{rec} values signify that the two resulting probe–target duplexes are much more stable than the Invader and target duplexes. Interestingly, all of the Invader duplexes studied herein display favorable binding energies for recognition of isosequential dsDNA targets (ΔG^{293}_{rec} between −29 and −5 kJ/mol; Table 2). Invader duplexes with energetic hotspots comprising exclusively **C** and/or **U** monomers display the most favorable binding energies (ΔG^{293}_{rec} between −29 and −24 kJ/mol; Table 2), which largely reflects the greater stabilization of probe–target duplexes when 2′-*O*-(pyren-1-yl)methyl-RNA monomers are flanked by 3′-purines. Concomitantly, Invader duplexes with hotspots exclusively comprising **A** and/or **G** monomers display the least favorable binding energies (ΔG^{293}_{rec} between −14 and −5 kJ/mol; Table 2). The binding energies of Invaders with other hotspots fall between these two extremes (ΔG^{293}_{rec} between −23 and −14 kJ/mol; Table 2). Importantly, these results indicate that incorporation of +1 interstrand zippers of 2′-*O*-(pyren-1-yl)methyl-RNA monomers is a general strategy to activate probes for dsDNA recognition.

Invader-Mediated Recognition of DNA Hairpins. The dsDNA recognition characteristics of four Invader duplexes—selected for their wide range of ΔG^{293}_{rec} and absolute T_m values—were evaluated using the electrophoretic mobility shift assay that we recently introduced and validated (Figure 2a).[29,31] Briefly described, digoxigenin (DIG)-labeled DNA hairpins (DHs) comprising 9-mer double-stranded stems linked via T_{10} loops serve as model dsDNA targets. The unimolecular nature of the hairpins confers extra stability to the stem region, which renders it a more challenging target than isosequential dsDNA targets [compare the T_m values of hairpins (Figure 2b) and isosequential dsDNA targets (Table 1)]. Invader-mediated recognition of DNA hairpins is expected to yield recognition complexes with lower electrophoretic mobilities on nondenaturing PAGE gels than DNA hairpins alone (Figure 2a).

Indeed, room-temperature incubation of Invader duplexes with their respective DNA hairpin targets results in dose-dependent formation of recognition complexes (Figure 2c–g). The results indicate that the ΔG^{293}_{rec} value and the dsDNA recognition efficiency are correlated. Thus, the Invader duplex with the greatest recognition potential (**ON9:ON12**, ΔG^{293}_{rec} = −29 kJ/mol; Table 2) results in ~80% recognition of **DH1** when used in 100-fold excess (Figure 2g), while **ON8:ON13**, which exhibits the lowest recognition potential (ΔG^{293}_{rec} = −5 kJ/mol; Table 2), hardly results in any recognition of **DH4** (Figure 2g). **ON6:ON15** and **ON10:ON11**, which were predicted to have intermediate recognition potentials (ΔG^{293}_{rec} = −24 and −19 kJ/mol, respectively; Table 2), display intermediate dsDNA recognition efficiencies (Figure 2g). It is interesting to note that dsDNA recognition is slightly more

dx.doi.org/10.1021/jo402085v | J. Org. Chem. 2013, 78, 12040–12048

Table 4. Thermal Denaturation Temperatures (T_m) and Deviation of Additivity (DA) Values of 14-Mer DNA Duplexes Modified with 2′-*O*-(Pyren-1-yl)methyl-RNA Monomers[a]

		T_m [ΔT_m] (°C)				
ON	Invader	upper strand vs ssDNA	lower strand vs ssDNA	Invader duplex	dsDNA target	DA (°C)
ON21 **ON22**	5′-T**U**A CTC A**C**G A**U**G CT 3′-AA**U** GAG TG**C** TA**C** GA	71.0 [+20.0]	68.0 [+17.0]	54.0 [+3.0]	51.0	−34.0
ON23 **ON24**	5′-T**U**A CT**C** ACG **A**TG CT 3′-AA**U** GAG **U**GC T**A**C GA	67.5 [+16.5]	63.5 [+12.5]	40.5 [−10.5]	51.0	−39.5
ON25 **ON26**	5′-TTA **C**TC A**C**G AT**G** CT 3′-AAT G**A**G TG**C** TAC **G**A	63.5 [+12.5]	61.0 [+10.0]	47.5 [−3.5]	51.0	−26.0
ON27 **ON28**	5′-TT**A** CTC **A**CG AT**G** CT 3′-AAT **G**AG T**G**C TAC **G**A	56.0 [+5.0]	54.0 [+3.0]	38.0 [−13.0]	51.0	−21.0

[a]See Table 1 for experimental conditions and definitions.

Table 5. Changes in Gibbs Free Energy upon Duplex Formation (ΔG^{293}) and Thermodynamic dsDNA-Targeting Potentials (ΔG^{293}_{rec}) of 14-Mer Invaders at 293 K[a]

		ΔG^{293}[$\Delta\Delta G^{293}$] (kJ/mol)				
ON	Invader	upper strand vs ssDNA	lower strand vs ssDNA	Invader duplex	dsDNA target	ΔG^{293}_{rec} (kJ/mol)
ON21 **ON22**	5′-T**U**A CTC A**C**G A**U**G CT 3′-AA**U** GAG TG**C** TA**C** GA	−74 ± 1 [−8]	−91 ± 0 [−25]	−58 ± 1 [+8]	−66 ± 1	−41
ON23 **ON24**	5′-T**U**A CT**C** ACG **A**TG CT 3′-AA**U** GAG **U**GC T**A**C GA	−83 ± 1 [−17]	−73 ± 1 [−7]	−45 ± 1 [+21]	−66 ± 1	−45
ON25 **ON26**	5′-TTA **C**TC A**C**G AT**G** CT 3′-AAT G**A**G TG**C** TAC **G**A	−78 ± 1 [−12]	−74 ± 1 [−8]	−48 ± 1 [+18]	−66 ± 1	−38
ON27 **ON28**	5′-TT**A** CTC **A**CG AT**G** CT 3′-AAT **G**AG T**G**C TAC **G**A	−68 ± 1 [−2]	−75 ± 1 [−9]	−47 ± 0 [+19]	−66 ± 1	−30

[a]See Table 2 for definitions and conditions.

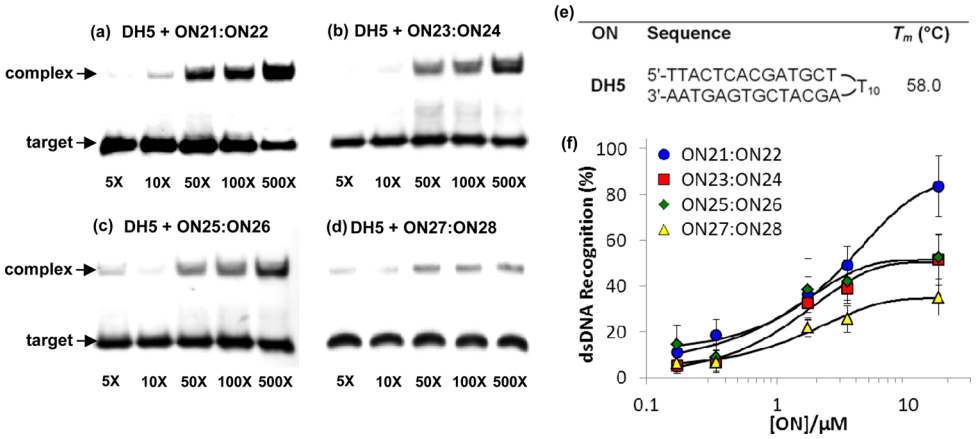

Figure 3. Invader-mediated recognition of DNA hairpins with 14-mer isosequential stem regions. (a−d) Gel electropherograms illustrating dose−response experiments between **DH5** and (a) **ON21**:**ON22**, (b) **ON23**:**ON24**, (c) **ON25**:**ON26**, and (d) **ON27**:**ON28**. (e) Sequence and T_m of DNA hairpin **DH5** (for conditions of thermal denaturation experiments, see Table 1). (f) Dose−response curves (see Figure 2 for experimental conditions).

efficient with the more strongly activated **ON6**:**ON15** compared with **ON10**:**ON11**, in spite of the significantly greater Invader (T_m = 41.5 vs 26.5 °C, respectively; Table 1) and duplex target (69.5 vs 59.0 °C, respectively; Figure 2b) thermostabilities. This indicates that Invader-mediated dsDNA recognition can occur at experimental temperatures that are considerably lower than the T_m values of the Invader and/or target duplexes, which is likely to prove important for biological applications where the experimental temperature is not easily adjustable.

Less than 40% recognition of **DH1** is observed when single-stranded **ON9** or **ON12** is used at 500-fold molar excess (Figure S8 in the Supporting Information), which demonstrates that both strands of Invader duplexes are needed to ensure efficient recognition of dsDNA. Moreover, incubation of Invader duplexes **ON9**:**ON12**, **ON6**:**ON15**, and **ON10**:**ON11** with DNA hairpins that feature fully base-paired but non-isosequential stem regions (i.e., one or two base pair deviations relative to the Invader probes) fails to produce significant amounts of recognition complexes even when the Invaders are used in 500-fold excess, which demonstrates that the recognition process proceeds with excellent fidelity (Figure 2h−j).

Properties of 14-Mer Invader Duplexes. Next, we set out to examine whether the design principles inferred from the 9-mer study can be applied to longer and more densely modified Invader duplexes. Toward this end, we designed four 14-mer Invaders, each modified with three energetic hotspots

that were dispersed in a similar manner and selected to afford differentially activated probes (see Table 4). For example, the three hotspots used in Invader duplex **ON21**:**ON22** comprise **C** and/or **U** monomers and were expected to strongly promote dsDNA recognition on the basis of the observed ΔG^{293}_{rec} values in the 9-mer model study (Table 2). Conversely, the three hotspots used in Invader duplex **ON27**:**ON28** comprise **A** and/or **G** monomers and therefore were expected to result in a less efficient probe. Invaders **ON23**:**ON24** and **ON25**:**ON26** were expected to fall between these two extremes.

The thermal denaturation data (Table 4) and thermodynamic data (Table 5) exhibit the expected trends with a couple of exceptions. **ON21** and **ON22** display the highest affinity toward ssDNA targets in this series, while **ON27** and **ON28** display the lowest affinity toward ssDNA targets (first two T_m columns in Table 4). The observed changes in Gibbs free energy upon duplex formation between individual probe strands and ssDNA corroborate these findings (first two ΔG^{293} columns in Table 5), except that **ON21**:ssDNA is less stable than expected. The Invader duplexes are destabilized relative to the reference duplexes. It should be noted that **ON21**:**ON22** is the most thermostable of the evaluated Invaders (see the ΔT_m and $\Delta\Delta G^{293}$ values in the "Invader duplex" columns in Tables 4 and 5, respectively). As a result, the dsDNA recognition potential decreases in the order **ON23**:**ON24** > **ON21**:**ON22** > **ON25**:**ON26** > **ON27**:**ON28** (see the ΔG^{293}_{rec} values in Table 5).

Incubation of these Invader duplexes with their DNA hairpin target **DH5** results in dose-dependent recognition of the mixed-sequence dsDNA stem region (GC content ∼43%) in all four cases, with **ON21**:**ON22** as the most efficient probe (50% recognition at ∼125-fold excess; Figure 3). It is noteworthy that even Invader **ON27**:**ON28** featuring less desirable energetic hotspots recognizes **DH5**, albeit with the lowest efficiency in this probe series. Importantly, this suggests that beneficial probe architectures can compensate for the effect of suboptimal energetic hotspots.

In summary, the design principles inferred from the 9-mer study can be confidently applied to longer and more densely modified Invader duplexes, but a systematic examination of the interplay between probe architecture (i.e., number and position of energetic hotspots) and dsDNA recognition efficiency is necessary to gain a more complete picture of Invader probe design. Studies along these lines are ongoing and will be presented in due course. Nonetheless, the results presented herein will already guide the design of efficient Invaders for recognition of mixed-sequence dsDNA.

CONCLUSION

The present study demonstrates that incorporation of +1 interstrand zippers of 2′-*O*-(pyren-1-yl)methyl-RNA monomers is a general approach toward activation of double-stranded oligodeoxyribonucleotide probes for recognition of mixed-sequence dsDNA targets. The recognition efficiency of the probes is, however, influenced by the composition of the energetic hotspots. Thus, Invader duplexes with hotspots comprising exclusively **C** and/or **U** monomers display very favorable dsDNA-binding affinities since (i) the resulting probe−target duplexes are most strongly stabilized when 2′-*O*-(pyren-1-yl)methyl-RNA monomers are flanked by 3′-purines (Tables 1 and 2) and (ii) probe−target stabilization is more important than Invader duplex destabilization in driving the favorable thermodynamics of dsDNA recognition (compare the relative contributions of probe−target duplexes to ΔG^{293}_{rec} relative to Invader duplexes; Table 2). Invaders with hotspots constructed using one or two **G** monomers (or two **A** monomers) are the least activated constructs for dsDNA recognition. However, a beneficial probe architecture can compensate for a suboptimal choice of energetic hotspots for construction of Invader duplexes (Figure 3). The insight gained from this study will guide the design of efficient dsDNA-targeting Invaders to enable applications in molecular biology, nucleic acid diagnostics, and biotechnology.

EXPERIMENTAL SECTION

2′-*O*-(Pyren-1-yl)methylguanosine (2). 1-Chloromethylpyrene (1.86 g, 7.41 mmol) was added to a suspension of guanosine (**1**) (3.00 g, 10.6 mmol) and NaH (60% suspension in mineral oil, 0.64 g, 26.5 mmol) in anhydrous DMSO. The reaction mixture was stirred for ∼14 h at room temperature, at which point water (100 mL) was added. The resulting solids were filtered off, washed with water (3 × 20 mL), and dried. The filtrate was extracted with EtOAc (3 × 50 mL), and the organic layer was dried (Na_2SO_4). The aqueous layer was partially evaporated (∼100 mL remaining) and left overnight at rt, which resulted in an additional crop of solids. The solids and organic layer were combined and purified by silica gel column chromatography (4−8% v/v MeOH in CH_2Cl_2) to afford an off-white residue, which was precipitated from acetone to afford nucleoside **2** (0.90 g, 24%) as a white solid. R_f = 0.3 (10% MeOH in CH_2Cl_2, v/v). MALDI-HRMS: *m*/*z* 520.1598 ($[M + Na]^+$, $C_{27}H_{23}N_5O_5Na^+$, calcd 520.1591). ^{1}H NMR (DMSO-d_6): δ 10.58 (s, 1H, ex, NH), 8.27−8.32 (m, 3H, Py), 8.01−8.21 (m, 6H, Py), 7.97 (s, 1H, H8), 6.38 (s, 2H, 2ex, NH_2), 5.97 (d, 1H, *J* = 6.7 Hz, H1′), 5.40−5.43 (m, 2H, 1 ex, 3′-OH, CH_2Py), 5.20−5.23 (d, 1H, *J* = 11.4 Hz, CH_2Py), 5.09 (t, 1H, ex, *J* = 5.2 Hz, 5′-OH), 4.61−4.64 (m, 1H, H2′), 4.43−4.47 (m, 1H, H3′), 4.00−4.03 (m, 1H, H4′), 3.63−3.68 (m, 1H, H5′), 3.57−3.61 (m, 1H, H5′). ^{13}C NMR (DMSO-d_6): δ 156.6, 153.6, 151.2, 135.3 (C8), 131.3, 130.65, 130.63, 130.2, 128.7, 127.30 (Py), 127.26 (Py), 127.1 (Py), 126.2 (Py), 125.23 (Py), 125.18 (Py), 124.4 (Py), 123.9, 123.7, 123.5 (Py), 116.7, 86.1 (C4′), 84.6 (C1′), 81.3 (C2′), 69.9 (CH_2Py), 69.0 (C3′), 61.3 (C5′).

2-*N*-Isobutyryl-2′-*O*-(pyren-1-yl)methylguanosine (3). Nucleoside **2** (0.26 g, 0.52 mmol) was dried through repeated coevaporation with anhydrous pyridine and redissolved in anhydrous pyridine (6 mL). Trimethylsilyl chloride (0.5 mL, 3.92 mmol) was added, and the reaction mixture was stirred for 2 h at rt. After the mixture was cooled to 0 °C, isobutyryl chloride (0.15 mL, 1.57 mmol) was added over 10 min with continued cooling. This mixture was then stirred for 3 h at rt and then cooled to 0 °C. Water (2 mL) was added, and the mixture was stirred at 0 °C for 10 min and then for another 5 min at rt, at which point aq. NH_3 (28%, 5 mL) was added. The resulting solution was stirred at rt for 15 min and evaporated to near dryness. The residual material was taken up in CH_2Cl_2 (100 mL) and washed with water (2 × 60 mL). The organic phase was dried (Na_2SO_4) and evaporated to dryness, and the resulting crude material was purified by silica gel column chromatography (1−3% v/v MeOH in CH_2Cl_2) to afford nucleoside **3** (220 mg, 74%) as a pale-yellow solid. R_f = 0.6 (10% v/v MeOH in CH_2Cl_2). MALDI-HRMS: *m*/*z* 590.2008 ($[M + Na]^+$, $C_{31}H_{29}N_5O_6Na^+$, calcd 590.2010). ^{1}H NMR (DMSO-d_6): δ 11.85 (s, 1H, ex, NH), 11.30 (s, 1H, ex, NH), 8.21−8.28 (m, 3H, Py), 8.19 (s, 1H, H8), 8.01−8.14 (m, 5H, Py), 7.94−7.97 (d, 1H, *J* = 7.8 Hz, Py), 5.94 (d, 1H, *J* = 6.7 Hz, H1′), 5.43−5.46 (m, 2H, 1 ex, 3′-OH, CH_2Py), 5.14−5.16 (d, 1H, *J* = 11.4 Hz, CH_2Py), 5.08 (t, 1H, ex, *J* = 5.2 Hz, 5′-OH), 4.65−4.68 (m, 1H, H2′), 4.46−4.48 (m, 1H, H3′), 4.01−4.03 (m, 1H, H4′), 3.57−3.67 (m, 2H, H5′), 2.56−2.61 (septet, 1H, *J* = 6.7 Hz, $CHMe_2$), 1.04 (d, 3H, *J* = 6.7 Hz, CH_3), 1.00 (d, 3H, *J* = 6.7 Hz, CH_3). ^{13}C NMR (DMSO-d_6): δ 179.8, 154.5, 148.5, 147.8, 137.2 (C8), 131.2, 130.62, 130.58, 130.1, 128.7, 127.3 (Py), 127.2 (Py), 127.07 (Py), 127.06 (Py), 126.1 (Py), 125.2 (Py), 125.1 (Py), 124.3 (Py), 123.8, 123.6, 123.5 (Py), 119.9, 86.5 (C4′), 84.7 (C1′), 81.6 (C2′), 70.2 (CH_2Py), 69.2 (C3′), 61.3 (C5′),

dx.doi.org/10.1021/jo402085v | J. Org. Chem. 2013, 78, 12040−12048

34.5 ($CHMe_2$), 18.7 (CH_3), 18.6 (CH_3). A trace impurity of CH_2Cl_2 was identified in the ^{13}C NMR spectrum of **3**.

5′-*O*-(4,4′-Dimethoxytrityl)-2-*N*-isobutyryl-2′-*O*-(pyren-1-yl)-methylguanosine (4). Nucleoside **3** (200 mg, 3.56 mmol) was coevaporated with anhydrous pyridine (3 × 1.5 mL) and redissolved in anhydrous pyridine (3 mL). To this was added 4,4′-dimethoxytrityl chloride (DMTrCl) (300 mg, 0.53 mmol) and *N*,*N*-dimethyl-4-aminopyridine (DMAP) (∼10 mg), and the reaction mixture was stirred at rt for ∼14 h. The reaction mixture was diluted with CH_2Cl_2 (20 mL), and the organic phase sequentially washed with water (2 × 10 mL) and sat. aq. $NaHCO_3$ (2 × 10 mL). The organic phase was evaporated to near dryness, and the resulting crude material was coevaporated with abs. EtOH and toluene (2:1 v/v, 3 × 2 mL) and purified by silica gel column chromatography (0−5% v/v MeOH in CH_2Cl_2) to afford nucleoside **4** (270 mg, 88%) as a pale-yellow foam. R_f = 0.8 (7% v/v MeOH in CH_2Cl_2). MALDI-HRMS: *m*/*z* 892.3325 ($[M + Na]^+$, $C_{52}H_{47}N_5O_8Na^+$, calcd 892.3317). ^1H NMR (DMSO-d_6): δ 11.90 (s, 1H, ex, NH), 11.34 (s, 1H, ex, NH), 8.25−8.32 (m, 3H, Py), 8.04−8.15 (m, 5H, Py), 8.03 (s, 1H, H8), 7.99−8.01 (d, 1H, *J* = 7.8 Hz, Py), 7.32−7.34 (m, 2H, DMTr), 7.19−7.25 (m, 7H, DMTr), 6.79−6.82 (m, 4H, DMTr), 5.97 (d, 1H, *J* = 5.5 Hz, H1′), 5.49−5.51 (d, 1H, *J* = 11.7 Hz, CH_2Py), 5.47 (d, 1H, ex, *J* = 5.4 Hz, 3′-OH), 5.22−5.25 (d, 1H, *J* = 11.7 Hz, CH_2Py), 4.72 (ap t, 1H, *J* = 5.5 Hz, H2′), 4.45−4.48 (m, 1H, H3′), 4.11−4.14 (m, 1H, H4′), 3.710 (s, 3H, CH_3O), 3.706 (s, 3H, CH_3O), 3.28−3.31 (m, 1H, H5′, overlap with H_2O signal), 3.18−3.22 (m, 1H, H5′), 2.63 (septet, 1H, *J* = 6.7 Hz, $CHMe_2$), 1.04−1.07 (2d, 6H, both *J* = 6.7 Hz, CH_3). ^{13}C NMR (DMSO-d_6): δ 179.8, 158.0, 154.5, 148.5, 147.9, 144.7, 137.1 (C8), 135.4, 135.3, 131.1, 130.7, 130.6, 130.1, 129.6 (DMTr), 128.7, 127.7 (DMTr), 127.6 (DMTr), 127.31 (Py), 127.29 (Py), 127.2 (Py), 127.0 (Py), 126.6 (DMTr), 126.2 (Py), 125.3 (Py), 125.2 (Py), 124.4 (Py), 123.9, 123.7, 123.5 (Py), 120.1, 113.1 (DMTr), 85.6, 85.1 (C1′), 84.2 (C4′), 80.8 (C2′), 70.3 (CH_2Py), 69.4 (C3′), 63.9 (C5′), 54.9 (CH_3O), 34.6 ($CHMe_2$), 18.8 (CH_3), 18.7 (CH_3).

3′-*O*-(2-Cyanoethoxy(diisopropylamino)phosphinyl)-5′-*O*-(4,4′-dimethoxytrityl)-2-*N*-isobutyryl-2′-*O*-(pyren-1-yl)-methylguanosine (5). Nucleoside **4** (260 mg, 0.29 mmol) was coevaporated with anhydrous 1,2-dichloroethane (2 × 2 mL) and redissolved in anhydrous CH_2Cl_2 (7 mL). To this was added anhydrous *N*,*N*-diisopropylethylamine (DIPEA) (213 μL, 1.19 mmol) and 2-cyanoethyl-*N*,*N*-diisopropylchlorophosphoramidite (PCl reagent) (133 μL, 0.59 mmol), and the reaction mixture was stirred at rt for ∼3 h, whereupon abs. EtOH (1 mL) and CH_2Cl_2 (20 mL) were sequentially added. The organic phase was washed with sat. aq. $NaHCO_3$ (10 mL) and evaporated to near dryness, and the resulting residue was purified by silica gel column chromatography (40−70% v/v EtOAc in petroleum ether) to afford the desired phosphoramidite **5** (250 mg, 78%) as a white foam. R_f = 0.8 (5% v/v MeOH in CH_2Cl_2). MALDI-HRMS: *m*/*z* 1092.4389 ($[M + Na]^+$, $C_{61}H_{64}N_7O_9P\ Na^+$, calcd 1092.4395). ^{31}P NMR ($CDCl_3$): δ 150.39, 150.35.

Synthesis and Purification of Modified ONs. The corresponding phosphoramidites of monomers **A**, **C**, and **U** (A^{Bz}, C^{Bz}, U) were obtained as previously described.[33,34] The phosphoramidite of monomer **G** was obtained as described above. Modified ONs were synthesized on an automated DNA synthesizer (0.2 μmol scale; succinyl-linked LCAA-CPG support) using a ∼50-fold molar excess of 2′-*O*-(pyren-1-yl)methyl-RNA phosphoramidites in anhydrous acetonitrile (at 0.02 M) and extended coupling (4,5-dicyanoimidazole as the activator, 15 min, ∼98% coupling yield) and oxidation (45 s). Standard protocols were used with DNA phosphoramidites. Cleavage from the solid support and removal of protecting groups was accomplished using 32% aq. ammonia (55 °C, 12 h). ONs were purified via ion-pair reversed-phase HPLC using a triethylammonium acetate buffer−water/acetonitrile (v/v) gradient, detritylated (80% aq. AcOH), and precipitated from acetone (−18 °C for 12−16 h). The identities of all modified ONs were verified through MALDI-MS/MS analysis recorded in positive ion mode on a quadrupole time-of-flight tandem mass spectrometer equipped with a MALDI source using anthranilic acid as a matrix (Table S1 in the Supporting Information). Purity (>90%) was verified by ion-pair reversed-phase HPLC running in analytical mode.

Thermal Denaturation Experiments. ON concentrations were estimated using the following extinction coefficients (OD/μmol) at 260 nm: dA (15.2), dC (7.05), dG (12.0), T (8.4), and pyrene (22.4). Quartz optical cells with a path length of 1.0 cm were used. Strands were mixed, denatured through heating to ∼70 °C, and cooled to the starting temperature of the experiment. Thermal denaturation curves (1.0 μM final concentration of each strand) were recorded on a Peltier-controlled UV/vis spectrophotometer using a medium salt buffer (100 mM NaCl, 0.1 mM EDTA, and pH 7.0 adjusted with 10 mM Na_2HPO_4 and 5 mM Na_2HPO_4). A temperature ramp of 0.5 °C/min was used in all of the experiments. Thermal denaturation temperatures (T_m) were determined as the maxima of the first derivatives of the denaturation curves. The experimental temperatures ranged from at least 15 °C below T_m (although not below 3 °C) to at least 20 °C above T_m. Reported T_m values are averages of at least two experiments within ±1.0 °C, unless otherwise mentioned.

Determination of Thermodynamic Parameters. Thermodynamic parameters for duplex formation were determined through baseline fitting of denaturation curves using the software provided with the UV/vis spectrometer. Bimolecular reactions, two-state melting behavior, and a heat capacity change of $\Delta C_p = 0$ upon hybridization were assumed.[46] A minimum of two experimental denaturation curves were each analyzed at least three times to minimize errors arising from baseline choice. Averages and standard deviations are listed.

Absorption Spectra. UV−vis absorption spectra (range: 300−400 nm) were recorded at 5 °C using the same samples and instrumentation as in the thermal denaturation experiments.

Steady-State Fluorescence Emission Spectra. Steady-state fluorescence emission spectra were recorded on a Peltier-controlled fluorimeter using the same samples as in the thermal denaturation experiments (i.e., in nondeoxygenated T_m buffer). Spectra were obtained as averages of five scans using an excitation wavelength of λ_{ex} = 350 nm, excitation slit = 5.0 nm, emission slit = 2.5 nm, and a scan speed of 600 nm/min. Spectra were recorded at 5 °C to ascertain maximal duplex formation.

Recognition of DNA Hairpins in Cell-Free Assay. This assay, which was chosen in lieu of footprinting experiments to avoid the use of ^{32}P-labeled targets, was performed in a similar manner as previously described.[29,31] Unmodified **DH1**−**DH5** were obtained from commercial sources and used without further purification. **DH1**−**DH5** were 3′-DIG-labeled using the second-generation DIG Gel Shift Kit (Roche Applied Bioscience) as recommended. The DIG-labeled ONs were diluted and used in the recognition experiments without further purification. Preannealed Invader duplexes (85 °C for 2 min, cooled to room temperature over 15 min) and DIG-labeled dsDNA targets (34.4 nM) were mixed and incubated in HEPES buffer (50 mM HEPES, 100 mM NaCl, 5 mM $MgCl_2$, 10% sucrose, 1.44 mM spermine tetrahydrochloride, pH 7.2) for 15 h at room temperature. The reaction mixtures were diluted with 6× DNA loading dye (Fermentas) and loaded onto a 12 or 16% nondenaturing polyacrylamide gel. Electrophoresis was performed using a constant voltage of 70 V for 2 h at ∼4 °C using 0.5× TBE (45 mM Tris, 45 mM boric acid, 1 mM EDTA) as a running buffer. Gels were blotted onto a positively charged nylon membrane (Roche Applied Bioscience) using a constant voltage of 100 V at ∼4 °C. The membranes were exposed to anti-digoxigenin-AP F_{ab} fragments as recommend by the manufacturer of the DIG Gel Shift Kit, transferred to a hybridization jacket, and incubated with the substrate (CSPD) in detection buffer for 10 min at 37 °C. The chemiluminescence of the formed product was captured on X-ray film, which was developed using an X-ray film developer. The resulting bands were quantified using a multi-imager equipped with appropriate software. Recognition efficiency was determined as the intensity ratio between the recognition complex band and the total lane. Averages of three independent experiments are reported along with standard deviations. Nonlinear regression was used to fit data points from dose−response experiments.

Definition of "Interstrand Zipper Arrangement". The following nomenclature describes the relative arrangement between

dx.doi.org/10.1021/jo402085v | J. Org. Chem. 2013, 78, 12040−12048

two monomers positioned on opposing strands in a duplex. The number *n* describes the distance measured in number of base pairs and has a positive value if a monomer is shifted toward the 5′-side of its own strand relative to a second reference monomer on the other strand. Conversely, *n* has a negative value if a monomer is shifted toward the 3′-side of its own strand relative to a second reference monomer on the other strand.

■ ASSOCIATED CONTENT

Supporting Information

General experimental section; MS data for modified ONs; representative thermal denaturation curves and absorption spectra; steady-state fluorescence emission spectra; absorption maxima for 14-mer probes and duplexes; and NMR spectra for nucleosides **2**–**5**. This material is available free of charge via the Internet at http://pubs.acs.org.

■ AUTHOR INFORMATION

Corresponding Author

*E-mail: hrdlicka@uidaho.edu. Phone: 208-885-0108.

Notes

The authors declare the following competing financial interest(s): Dr. Hrdlicka is the inventor of intellectual property involving the Invader technology.

■ ACKNOWLEDGMENTS

This study was supported by Award R01 GM088697 from the National Institute of General Medical Sciences, National Institutes of Health; Awards IF13-001 and IF14-012 from the Higher Education Research Council, Idaho State Board of Education; and Minitube of America. We thank Dr. Lee Deobald (EBI Murdock Mass Spectrometry Center, University of Idaho) for assistance with mass spectrometric analysis and Dr. Carolyn Bohach (Food Science, University of Idaho) for access to gel documentation stations.

■ REFERENCES

(1) Simon, P.; Cannata, F.; Concordet, J.-P.; Giovannangeli, C. *Biochimie* **2008**, *90*, 1109–1116.
(2) Ghosh, I.; Stains, C. I.; Ooi, A. T.; Segal, D. J. *Mol. BioSyst.* **2006**, *2*, 551–560.
(3) Jensen, N. M.; Dalsgaard, T.; Jakobsen, M.; Nielsen, R. R.; Sørensen, C. B.; Bolund, L.; Jensen, T. G. *J. Biomed. Sci.* **2011**, *18*, No. 10.
(4) Rogers, F. A.; Lloyd, J. A.; Glazer, P. M. *Curr. Med. Chem.: Anti-Cancer Agents* **2005**, *5*, 319–326.
(5) Duca, M.; Vekhoff, P.; Oussedik, K.; Halby, L.; Arimondo, P. B. *Nucleic Acids Res.* **2008**, *36*, 5123–5138.
(6) Mukherjee, A.; Vasquez, K. M. *Biochimie* **2011**, *93*, 1197–1208.
(7) Kaihatsu, K.; Janowski, B. A.; Corey, D. R. *Chem. Biol.* **2004**, *11*, 749–758.
(8) Nielsen, P. E. *Curr. Opin. Mol. Ther.* **2010**, *12*, 184–191.
(9) Dervan, P. B.; Edelson, B. S. *Curr. Opin. Struct. Biol.* **2003**, *13*, 284–299.
(10) Vaijayanthi, T.; Bando, T.; Pandian, G. N.; Sugiyama, H. *ChemBioChem* **2012**, *13*, 2170–2185.
(11) Lohse, J.; Dahl, O.; Nielsen, P. E. *Proc. Natl. Acad. Sci. U.S.A.* **1999**, *96*, 11804–11808.
(12) Ishizuka, T.; Yoshida, J.; Yamamoto, Y.; Sumaoka, J.; Tedeschi, T.; Corradini, R.; Sforza, S.; Komiyama, M. *Nucleic Acids Res.* **2008**, *36*, 1464–1471.
(13) Aiba, Y.; Sumaoka, J.; Komiyama, M. *Chem. Soc. Rev.* **2011**, *40*, 5657–5668.
(14) Rapireddy, S.; Bahal, R.; Ly, D. H. *Biochemistry.* **2011**, *50*, 3913–3918.
(15) Bahal, R.; Sahu, B.; Rapireddy, S.; Lee, C.-M.; Ly, D. H. *ChemBioChem* **2012**, *13*, 56–60.
(16) Bogdanove, A. J.; Voytas, D. F. *Science* **2011**, *333*, 1843–1846.
(17) Gaj, T.; Gersbach, C. A.; Barbas, C. F., III. *Trends Biotechnol.* **2013**, *31*, 397–405.
(18) Kutyavin, I. V.; Rhinehart, R. L.; Lukhtanov, E. A.; Gorn, V. V.; Meyer, R. B., Jr.; Gamper, H. B., Jr. *Biochemistry* **1996**, *35*, 11170–11176.
(19) Tse, W. C.; Boger, D. L. *Chem. Biol.* **2004**, *11*, 1607–1617.
(20) Filichev, V. V.; Vester, B.; Hansen, L. H.; Pedersen, E. B. *Nucleic Acids Res.* **2005**, *33*, 7129–7137.
(21) Rusling, D. A.; Powers, V. E. C.; Ranasinghe, R. T.; Wang, Y.; Osborne, S. D.; Brown, T.; Fox, K. *Nucleic Acids Res.* **2005**, *33*, 3025–3032.
(22) Ge, R.; Heinonen, J. E.; Svahn, M. G.; Mohamed, A. J.; Lundin, K. E.; Smith, C. I. E. *FASEB J.* **2007**, *21*, 1902–1914.
(23) Beane, R.; Gabillet, S.; Montaillier, C.; Arar, K.; Corey, D. R. *Biochemistry* **2008**, *47*, 13147–13149.
(24) Hari, Y.; Obika, S.; Imanishi, T. *Eur. J. Org. Chem.* **2012**, 2875–2887.
(25) Hamilton, P. L.; Arya, D. P. *Nat. Prod. Rep.* **2012**, *29*, 134–143.
(26) Moreno, P. M. D.; Geny, S.; Pabon, Y. V.; Bergquist, H.; Zaghloul, E. M.; Rocha, C. S. J.; Oprea, I. I.; Bestas, B.; Andaloussi, S. E. L.; Jørgensen, P. T.; Pedersen, E. B.; Lundin, K. E.; Zain, R.; Wengel, J.; Smith, C. I. E. *Nucleic Acids Res.* **2013**, *41*, 3257–3273.
(27) Hrdlicka, P. J.; Kumar, T. S.; Wengel, J. *Chem. Commun.* **2005**, 4279–4281.
(28) Sau, S. P.; Kumar, T. S.; Hrdlicka, P. J. *Org. Biomol. Chem.* **2010**, *8*, 2028–2036.
(29) Didion, B. A.; Karmakar, S.; Guenther, D. C.; Sau, S.; Verstegen, J. P.; Hrdlicka, P. J. *ChemBioChem* **2013**, *14*, 1534–1538.
(30) Denn, B.; Karmakar, S.; Guenther, D. C.; Hrdlicka, P. J. *Chem. Commun.* **2013**, *49*, 9851–9853.
(31) Sau, S. P.; Madsen, A. S.; Podbevsek, P.; Andersen, N. K.; Kumar, T. S.; Andersen, S.; Rathje, R. L.; Anderson, B. A.; Guenther, D. C.; Karmakar, S.; Kumar, P.; Plavec, J.; Wengel, J.; Hrdlicka, P. J. *J. Org. Chem.* **2013**, *78*, 9560–9570.
(32) Crothers, D. M. *Biopolymers* **1968**, *6*, 575–584.
(33) Nakamura, M.; Shimomura, Y.; Ohtoshi, Y.; Sasa, K.; Hayashi, H.; Nakano, H.; Yamana, K. *Org. Biomol. Chem.* **2007**, *5*, 1945–1951.
(34) Karmakar, S.; Anderson, B. A.; Rathje, R. L.; Andersen, S.; Jensen, T.; Nielsen, P.; Hrdlicka, P. J. *J. Org. Chem.* **2011**, *76*, 7119–7131.
(35) Ti, G. S.; Gaffney, B. L.; Jones, R. A. *J. Am. Chem. Soc.* **1982**, *104*, 1316–1319.
(36) Asanuma, H.; Fujii, T.; Kato, T.; Kashida, H. *J. Photochem. Photobiol., C* **2012**, *13*, 124–135.
(37) Steady-state fluorescence emission spectra of single-stranded **ON1**–**ON20** and their corresponding duplexes with ssDNA were not conclusive in identifying pyrene binding modes (Figures S3–S6 in the Supporting Information).
(38) Yamana, K.; Iwase, R.; Furutani, S.; Tsuchida, H.; Zako, H.; Yamaoka, T.; Murakami, A. *Nucleic Acids Res.* **1999**, *27*, 2387–2392.
(39) Nakamura, M.; Fukunaga, Y.; Sasa, K.; Ohtoshi, Y.; Kanaori, K.; Hayashi, H.; Nakano, H.; Yamana, K. *Nucleic Acids Res.* **2005**, *33*, 5887–5895.
(40) Dioubankova, N. N.; Malakhov, A. D.; Stetsenko, D. A.; Gait, M. J.; Volynsky, P. E.; Efremov, R. G.; Korshun, V. A. *ChemBioChem* **2003**, *4*, 841–847.
(41) Hrdlicka, P. J.; Babu, B. R.; Sørensen, M. D.; Wengel, J. *Chem. Commun.* **2004**, 1478–1479.
(42) Seela, F.; Ingale, S. A. *J. Org. Chem.* **2010**, *75*, 284–295.
(43) Haner, R.; Garo, F.; Wenger, D.; Malinovskii, V. L. *J. Am. Chem. Soc.* **2010**, *132*, 7466–7471.
(44) Wojciechowski, F.; Lietard, J.; Leumann, C. J. *Org. Lett.* **2012**, *14*, 5176–5179.
(45) Winnik, F. M. *Chem. Rev.* **1993**, *93*, 587–614.
(46) Mergny, J. L.; Lacroix, L. *Oligonucleotides* **2003**, *13*, 515–537.